Metallographic characterisation of Al6061-T6 aluminium plates subjected to ballistic impact

A. Manes *, M. Pagani, M. Saponara, D. Mombelli, C. Mapelli, M. Giglio

Politecnico di Milano, Department of Mechanical Engineering, Via La Masa 1, 20156 Milan, Italy

Received 3 February 2014
Received in revised form
10 April 2014
Accepted 15 April 2014
Available online 26 April 2014

1. Introduction

Ballistic impacts, and other types of high-speed loading conditions, can be a relevant issue for several structural applications. Most research activities in the field of ballistic impacts have been devoted to experimental tests and to the creation of numerical models. Both approaches are aimed at analysing the performance of the target (or of the impactor) in terms of damage, penetration and residual velocity. Structural changes during penetration are investigated both for bullets and targets, but the microstructural modifications are usually not deeply explored. Actually, the scientific literature on the physical and structural changes of the materials involved during ballistic penetration is not extensive, particularly for aluminium-based alloys.

Aluminium plates are widely applied in lightweight systems where the weight is an important design criterion but ballistic steel is generally chosen for protection applications. However, Børvik et al. [1] showed the weight of a potential aluminium protection could approximately be 25% less than for an equally strong steel structure, thus indicating a better energy absorption attitude. Experimental studies regarding the behaviour of aluminium subjected to high-velocity impact were conducted to investigate the material response [2–9]. These analyses show that the effect of the projectile nose on the target plates varies as a function of significant parameters such as thickness, impact velocities and nose angle or bullet radius. However, even if the impacts between projectile and plates have been investigated, a detailed and extensive metallurgical and metallographic description of the impact phenomena has not been performed in detail and is the main aim of the present paper.

Material modification during impact is a complex phenomenon that involves localised phenomena that profoundly modify the microstructure of the material itself and its mechanical behaviour. A complex mix of fusion and failure drives the penetration of the bullets. Moreover adiabatic heating associated with thermal softening (in competition with hardening due to strain rate) causes extreme strain localisation along certain narrow bands, called *adiabatic shear bands* (ASB), as also investigated by [10–13]. Several phenomena clearly happen and an overview of their effect is of interest for a better physical comprehension. Damage mechanism, deformation and fracture behaviour as well as microstructural characteristics of a high-strength aluminium alloy (Al 2139) have

* Corresponding author.
E-mail address: andrea.manes@polimi.it (A. Manes).

Table 1
Chemical composition of Al6061-T6.

Al (%)	Mg (%)	Si (%)	Fe (%)	Cu (%)	Mn (%)	Cr (%)	Zn (%)	Ti (%)
98	0.8–1.2	0.4–0.8	0.7	0.15–0.4	0.15	0.04–0.35	0.25	0.15

been investigated under dynamic condition [14,15]. In these papers investigations point out the importance of the microstructure of the Al 2139 (grain size and morphology, dispersed particle and inclusions, precipitates), resulting in a favourable behaviour of the material to projectile penetration.

In the present study Al6061-T6 plates subjected to the impact of two 7.62 Armour Piercing projectiles types were investigated. The projectiles are composed of a steel core and a tungsten core, respectively. In Section 2 a description of the main mechanical properties of the Al6061-T6 is reported in order to increase the understanding of the impact behaviour and the modifications subsequently described. In Section 3 a brief description of the impact tests is presented. It is worth to mention that this study belongs to a wider research activity; a more detailed description of experimental tests and application of predictive models (analytical and numerical) has been reported in a recent article [16]. Section 4 is the core of the article: damage features are investigated along the entire penetration channels. Microstructural investigations have been carried out using optical and scanning electron microscopy. Firstly material modifications have been investigated in Sections 4.1 and 4.2. Adiabatic shear bands are identified and microhardness tests were performed to evaluate the localised mechanical property modifications near the impact areas. An indentation technique allows the local determination (in different points of the target at various distances from the penetration channel) of the strength properties of the material, indicating the effect of strain rate hardening and/or thermal softening [17]. However the influences of the penetration depth and of the bullet properties have been determined also by means of optical microscopy (OM) and scanning electron microscopy (SEM). The experimental research data is presented sequentially for tools of investigation. Finally, Section 5 contains the conclusions of the study.

2. Material

Al6061-T6 alloy belongs to the aluminium series 6000 alloyed by silicon and magnesium as the main alloying elements. These alloys are developed for solution quenching followed by an aging heat treatment. The aging heat treatment applied in the present case is defined as T6 in the EN technical standard. This alloy features good formability, workability, weldability and machinability. The chemical composition of Al6061-T6 is reported in Table 1. In order to evaluate the behaviour of the material during a ballistic impact, a material characterisation is fundamental. The material in the area involved by the impact can experience high deformation and damage; moreover the plastic flow varies significantly as a function of strain rate and temperature. Although the creation of numerical models is not the aim of this study, some data about the mechanical behaviour of the target material are useful to increase the understanding of the physical phenomenon of the penetration.

The constitutive relation of JC has been chosen to describe the plastic behaviour of the investigated alloy (Eq. (1)):

$$\sigma = [A + B(\varepsilon_p)^n]\left[1 + C\ln\left(\frac{\dot{\varepsilon}_p}{\dot{\varepsilon}_0}\right)\right]\left[1 - \left(\frac{T - T_a}{T_f - T_a}\right)^m\right] \quad (1)$$

where A is the elastic limit, B and n are characteristic constants of the plastic behaviour, C expresses the sensitivity to the strain rate,

Table 2
Material parameters of aluminum Al6061-T6.

ρ (kg/m^3)	2700
E (MPa)	70,000
ν	0.33
A (MPa)	270
B (MPa)	154.3
n	0.2215
C	0.1301
$\dot{\varepsilon}_0$ (s^{-1})	597.2
m	1.34
T_m (K)	925

$\dot{\varepsilon}_0$ is the reference strain rate (typically set to 1 s^{-1}), ε_p and $\dot{\varepsilon}_p$ are respectively plastic strain and plastic strain rate, T, T_a, T_f are respectively the actual temperature, i.e. room temperature and melting temperature in the absolute scale, m is the material constant for the temperature dependency. The constants A, B and n, reported in Table 2, have been obtained through a series of tensile tests supported by numerical models based on the inverse method [18]. The behaviour of this aluminium alloy at a high strain rate has been recently investigated in [19]: up to 10^3 s^{-1} the strain rate fails to show any significant influence on the hardening behaviour. However, this alloy exhibits a significant increase in the material strength for strain rates higher than 10^3 s^{-1} which is usually identified as an effect of the change in the dislocation motion mechanism [20]. Thus, both C and $\dot{\varepsilon}_0$ have been optimised to match the obtained experimental values, performed in a strain rate range between 10^{-4} and 10^4 s^{-1}. Although this behaviour is different from the data used in the past to represent ballistic response of 6061-T6, several authors have recently shown that the mechanical behaviour of aluminium alloys shows a low strain rate sensitivity in the range of an intermediate strain rate (up to about 10^3 s^{-1}) combined with a steep increase in the flow stress at higher values of the strain rate with a sensitivity of the parameter to heat treatment and grain size of the material [21–23]. Specifically for 6061-T6, several authors [19–22] have found a bilinear effect with a steep increase in the range of 10^3–10^4 s^{-1}. It is worth mentioning that the calibration carried out in [19], and reported in Table 2, has been performed with an FEM based optimisation of the experimental data. FEM models are comprehensive of the temperature increment due to adiabatic heating caused by the conversion of a part of plastic deformation into heat. Finally, the influence of temperature has been introduced using the values published in the literature by Lesuer et al. [20], see Table 2.

The calibration of the JC constants gives important information about the dependence of hardening on the strain-rate and temperature. In Fig. 1 the dynamic hardening promoted by the strain-rate increase and the thermal softening have been pointed out. As expected, at higher strain rates the flow stress increases; however, the effect of the temperature is very pronounced and an increase of 300 K leads to a decrease of the flow stress by about 50%. During the penetration process the local temperature may increase considerably due to plastic deformation and to the very short duration time of contact. Such effects are significant for the studied phenomena [24]; their effect will be shown also hereafter by means of micro-indentation analyses.

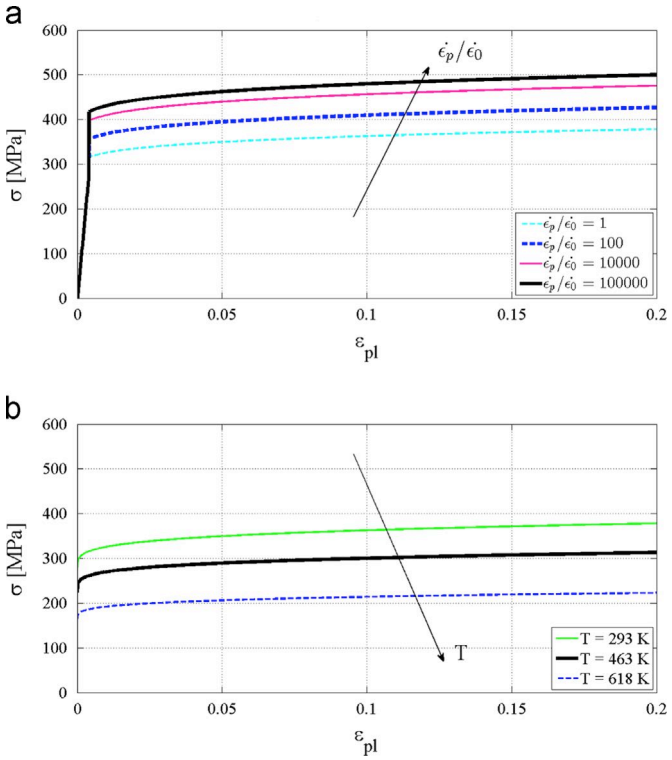

Fig. 1. Flow stress of Al6061-T6: (a) dynamic hardening at high strain-rate and (b) softening due to high temperature.

3. Experimental tests

A more detailed description on tests and results are reported in [16]; however a brief description is herein reported for the subject useful for the present investigation. Ballistic tests have been carried out on Al6061-T6 plates. Three thicknesses have been considered:

- 25 mm in order to have a complete perforation;
- 101.6 mm (4 in.) resulting in deep penetration of the whole bullet without causing the perforation of the plate: this condition allows regarding the target as a body of semi-infinite thickness [25];
- an intermediate thickness chosen as 76.2 mm (3 in.) to study an intermediate condition compared with the two former conditions.

At each single plate, consisting of an area of 300×600 mm^2, two shots have been fired. Two types of 7.62 mm Armour Piercing ammunitions were used:

- a steel penetrator with ogival shape encased in a copper jacket (Fig. 2a) with a mass of 9.28 g;
- a tungsten carbide penetrator (with a conical shape) encased in a brass sabot (CuZn30)(Fig. 2b), with a global mass of 11.6 g (5.1 g for the tungsten carbide core).

The set-up of the experiments consists in a conventional gun followed by laser detectors to measure the projectiles' initial velocity. Steel core bullets are shot at an average velocity of 771 m/s and tungsten carbide bullet at 742 m/s. Both bullets are supposed to have a spin of 750 rounds per minute. The target plate is placed at a distance of about 46 m from the gun, in order to allow a stabilisation of the trajectory, thus reducing the total yaw angle due to the external ballistic. The test set-up is similar to the one used for V50 ballistic test for armour [26]: the layout consists in a weapon, a velocity measurement equipment and target plates mounted over a test sample mount. However aim of this test programme is not to investigate in ballistic limit of the plates.

Both projectiles are much stronger than the plate alloy, but for the tungsten carbide bullet this assumption is true only for the core (this condition will be discussed in the results section).

3.1. Results

25 mm plates were completely perforated by both bullet types; however the steel core bullet passed through the thickness of the plate in its whole length, whereas the tungsten carbide core impact is characterised by brass sabot detachment that remains inside the hole. The 76.2 mm and the 101.6 mm plates were incompletely perforated and all bullets stopped their motion inside the plate thickness, see Fig. 3 and Table 3. Particularly, for the shot against the 101.6 mm plate, the 7.62 tungsten carbide core caused a ricochet effect (rebound of the bullet). Residual velocity following deep penetration was measured by means of sand penetration only for the 25 mm plate, and thus the result is approximate (Table 3). According to Bless et al. [27] the penetration velocity decay into sand has an approximately linear behaviour. The penetration depth of the two shots with the two bullet types without any target was preliminary acquired. The results were then correlated with a linear model that allows identifying the residual velocity using the penetration depth reached by the two bullets after the complete perforation of the 25 mm plate. However, the AP steel bullet remains the same both in the reference shot and in the test shot, whereas the tungsten carbide core bullet loses the sabot during the impact against the target; thus the residual mass and energy are lower and 200 m/s is considered to be the lower limit value.

The damage mechanisms shown by the targets clearly indicate that the projectiles mainly cause ductile hole enlargement. The difference between the two penetrators is evident mainly due to the presence of a relatively weak brass sabot of the tungsten carbide penetrator; the damage morphology is discussed in detail in the following sections. All the results show that the bullets remain substantially undeformed (except for the brass sabot). Fig. 4 shows the recovered bullets for the 25 mm plate impact (a), (b) and for 101.6 mm plate (c). The steel core bullet (both core and jacket) (Fig. 4a) does not undergo any visible deformation during the impact. The tungsten carbide core also remains undeformed (Fig. 4b) whereas the brass sabot usually separates and suffers extensive deformation. An exception is the shoot against the 101.6 mm plate, in which no separation of the sabot from the core takes place and the entire bullet rebounds (Fig. 4c).

4. Metallographic analyses

4.1. Microstructural investigation

Electrochemical etching to reveal the microstructure has been performed on ground and polished surfaces exploiting Barker's reagent [28] in polarised light observations.

Fig. 5 shows the microstructure of a 25 mm Al6061-T6 plate prior to a ballistic impact. The microstructural analysis demonstrates the typical features of this kind of aluminium alloy: large crystalline grains surrounded by Mg_2Si precipitates. As usual, such precipitates formed also inside the grains and they are intentionally induced to increase the material mechanical properties by the phenomena called “age hardening”. The precipitation mechanism and the effect of thermal treatment on precipitates fraction and morphology were well investigated in several studies and no in-

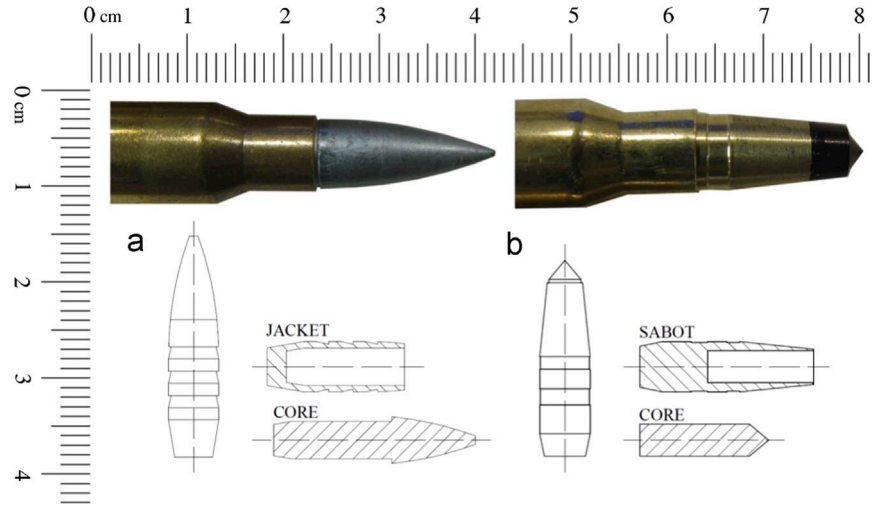

Fig. 2. 7.62 projectiles: (a) steel core and (b) tungsten carbide core.

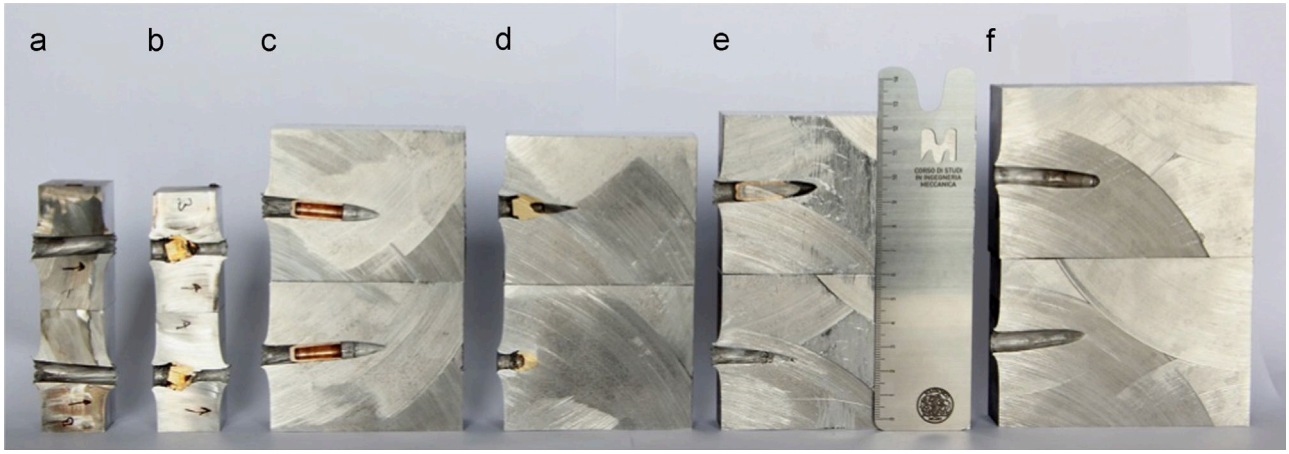

Fig. 3. General view of the cut plates/plate thickness: 25 mm (a, b), 76.2 mm (c, d), 101.6 mm (e, f); bullet type: steel core (a, c, e), tungsten carbide core (b, d, f).

Table 3
Experimental depth of penetration and residual velocity for the three plates.

Bullet type	Plate thickness [mm]	Experimental depth of penetration [mm]	Experimental residual velocity [m/s]
Steel core	25	–	≈ 500
	76.2	46.35	–
	101.6	46.45	–
Tungsten core	25	–	≈ 200
	76.2	38.11	–
	101.6	41.29	–

depth analyses are reported herein, since they are not the main topic of this research [29–33]. The crystalline grains are elongated along the rolling direction as the plates are rolled products. The presence of recrystallised grains resulting from plastic deformation and heat treatment processes is also shown. The shooting tests are performed hitting the plate surface orthogonally to the rolling direction, thereby allowing easy identification of the localised effects of the bullet penetration.

After the ballistic impact the microstructures near the impact areas feature large modifications of their morphology: the grains are stretched along the hole edge from the entry to the exit of bullets (Fig. 6a and c). This phenomenon is caused by the high material deformation due to the projectile crossing. Far from the

Fig. 4. Recovered bullets: (a) steel bullet and (b) tungsten carbide (only core) recovered after impact against 25 mm plate, (c) tungsten carbide bullet (core and brass sabot) recovered after ricochet effect against 101.6 mm plate.

bullet impact area (at 25 mm from the hole axis), the microstructures remain practically unaffected (Fig. 6b and d). These results confirm that the interaction between the bullet and the plate is

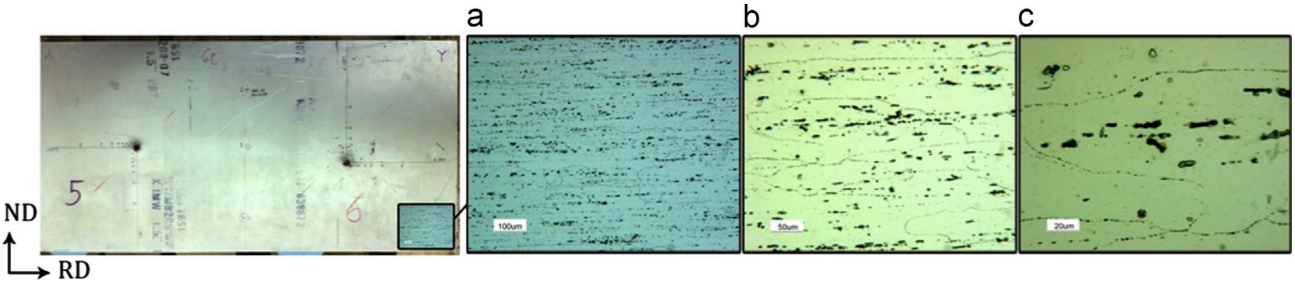

Fig. 5. Al6061-T6 microstructure with indicated RD (rolling direction) and NR (normal to rolling direction) reference system. Magnifications: (a) 100 × , (b) 200 × , (c) 500 × .

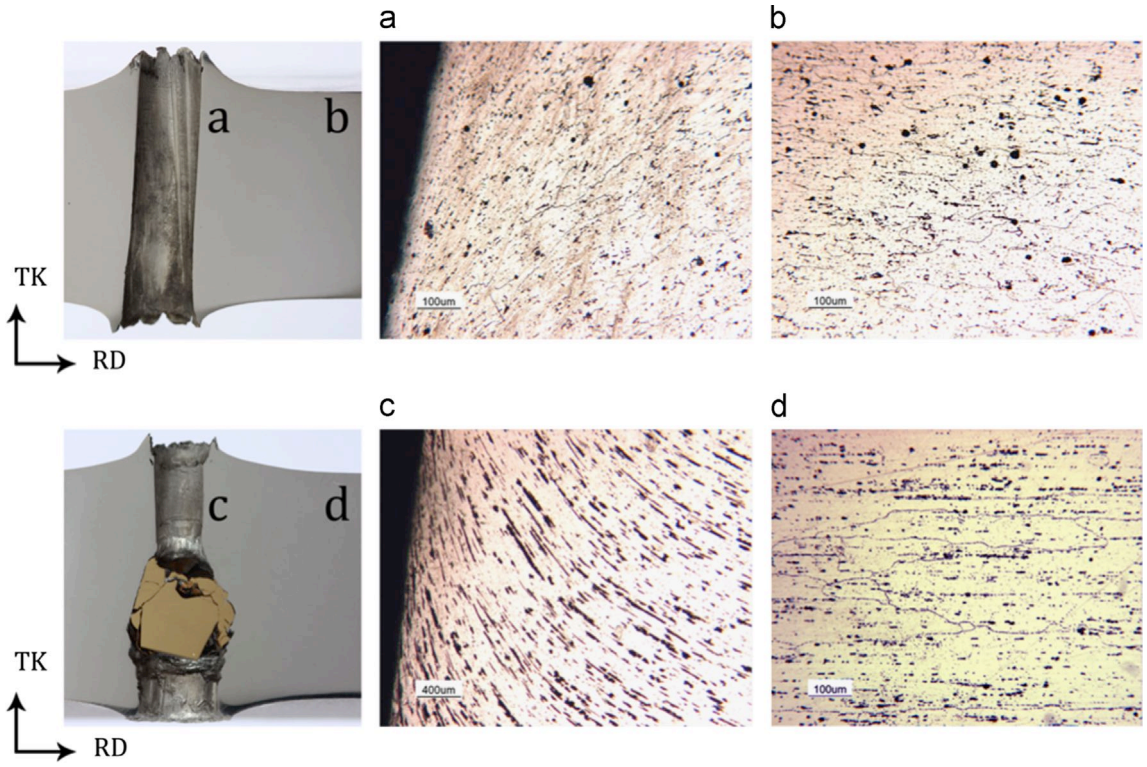

Fig. 6. Al6061-T6 micro-etching after the steel core bullet impact (impact direction is from below to top) – (a) near the bullet penetration channel and (b) far from the bullet penetration channel. Micro-etching after the tungsten core bullet impact – (c) near the bullet penetration channel and (d) far from the bullet penetration channel.

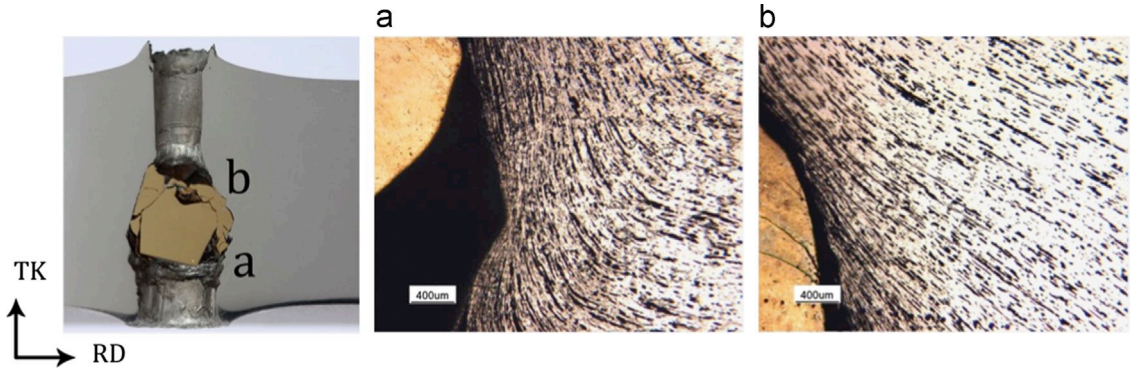

Fig. 7. Adiabatic shear bands along the channel edge of the tungsten core bullet impact: (a) entry side and (b) exit side.

limited to an area of only a few micrometres, in close proximity to the projectile hole.

The optical microscope investigation allows the identification of the *adiabatic shear bands* (ASB) along the hole edge, which typically form in materials subjected to high-velocity impacts, as described in [11–13]. Adiabatic shear bands (ASB) are generally considered as resulting from a thermo-mechanical instability leading to large deformation and high temperature in a narrow band, typically a few tens of micrometres in width [34–37]. The development of ASB is assumed to proceed in three steps: in stage I, the deformation in shear is homogeneous, and strain hardening of the material overcomes thermal softening effects; in stage II,

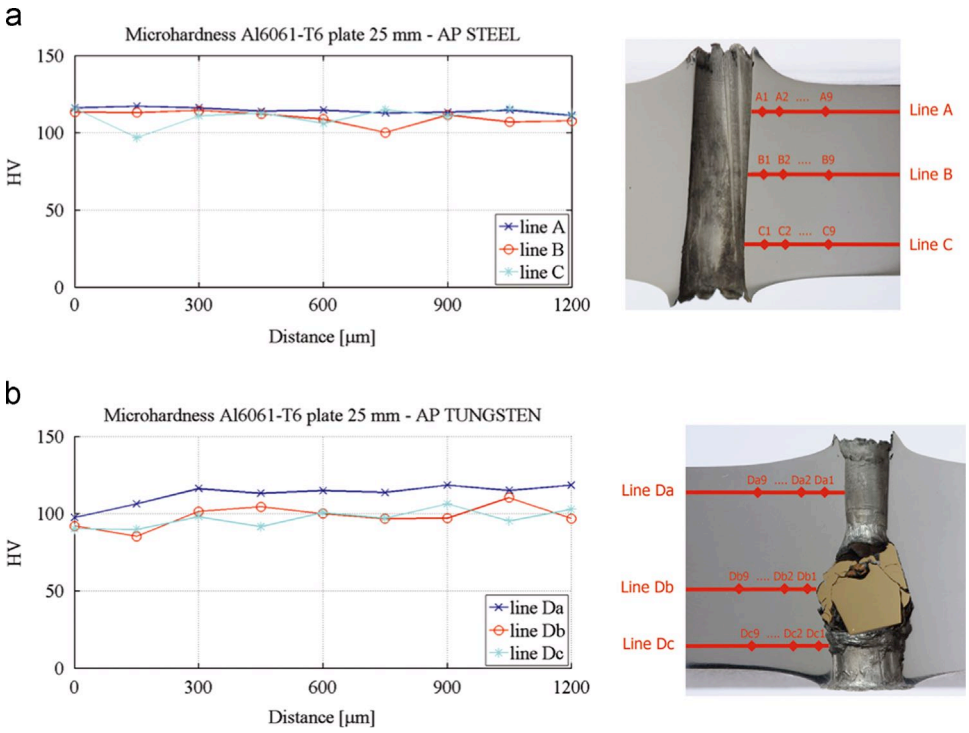

Fig. 8. Hardness trend for the 25 mm specimen impacted by (a) steel core projectile and (b) tungsten carbide core projectile; impact direction is from below to top.

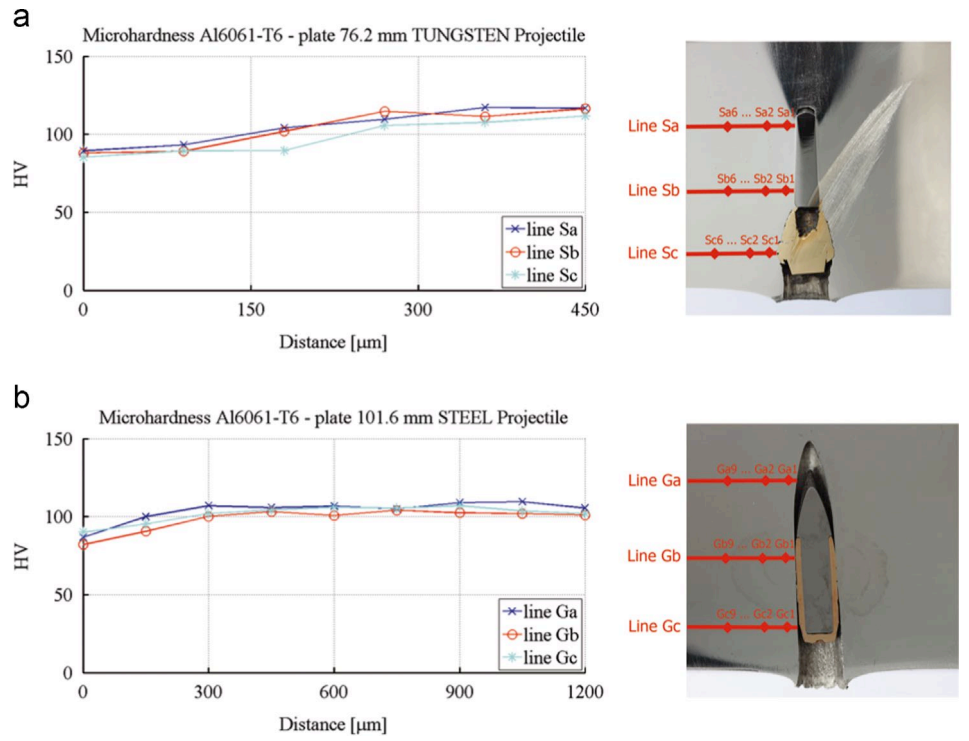

Fig. 9. Hardness trend for (a) 76.2 mm specimen impacted by the tungsten core projectile and (b) 101.6 mm specimen impacted by the steel core projectile.

after the maximum stress has been reached, a diffuse instability develops due to the prominence of thermal softening, and the deformation begins to be slightly heterogeneous; in stage III, a strong instability develops and deformation localises in a narrow band. Thus, ASB form when the thermal softening due to localised heat development competes with strain hardening and strain rate hardening. Due to the high speed of the bullet the heat generated in some slip planes (that usually induces significant softening) has insufficient time to dissipate. Besides the thermal effect, the hydrodynamic erosion and wear at the hole resulting from the impact induce high strain rate associated with high hardening, which balance the thermal softening, causing a non-homogenous

deformation resulting in a set of bands tilted with respect to the trajectory. Because the adiabatic shear bands are usually generated in a very short time, the shear bands undergo instantaneous heating and then are cooled rapidly by the relatively cool matrix around. The microstructure within the shear bands is different from the one in the matrix: in extreme case, such as bullet impact, dynamic recovery or dynamic recrystallisation may occur, resulting in a unique microstructure [37]. ASB are typical of ballistic impacts and may promote the developing of cracks. For instance in [38] ASB appear and produce cracks during a ballistic impact on austenitic steel, potentially resulting in failure before the fracture energy measured in slow tensile test is achieved. As discussed in [39] one of the reasons that make aluminium alloys good candidates for ballistic protection is their good thermal conductivity rendering them less sensitive to ASB. Actually, the ASB found in the present research do not show any presence of cracks originated from the bands. However, the identified ASB are quite different as a function of the bullet type: for the tungsten core projectile, the shear bands are more visible and intense than in the case of the steel core bullet (Fig. 6a and c). Moreover the final part of the penetration channel and the exit hole of the tungsten carbide core bullet show a ductile hole enlargement penetration with a cup-shaped exit hole that suggests plug failure. This type of failure is compatible with the conical shape of the tungsten carbide core whose tip is not very pronounced (the ratio diameter over height of the only tip is 5/3), thus resembling a blunt head bullet. As clearly known blunt projectiles have a perforation process that is controlled by ASB that generate plugging.

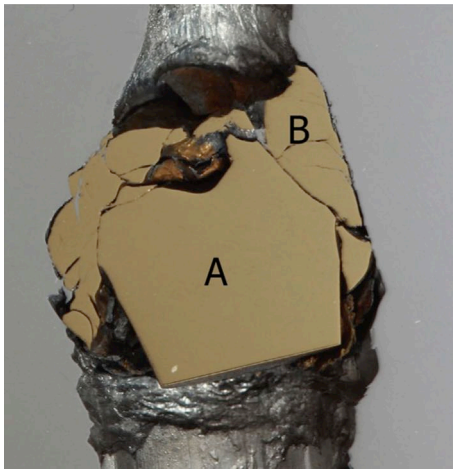

Fig. 10. Micro-hardness tests on brass sabot of the AP tungsten carbide core projectile. Indication of the two different zones.

The penetration channel of the tungsten core bullet impact, formed by the compression caused by the arrest of sabot, is an interesting feature (Fig. 7). The microstructure deformation is finer and features a higher density of adiabatic shear bands caused by the sabot lock-off inside the hole and the complete crossing of the tungsten core. A plausible explanation of this phenomenon is represented by the different magnitudes of absorbed energy. An ample deformation of the plate and the sabot as well as the friction effect highlighted in the following sections cause a highly localised temperature increase (adiabatic phenomena) and the material mechanical resistance decrease. This phenomenon is associated with the huge presence of ASB types and it is less pronounced in the steel core case with respect to the tungsten carbide core penetration. In both situations, the formed ASB seem to belong to the “transformed band” typology, since it is impossible to distinguish the boundary grains after the bullet impact [40].

4.2. *Micro-hardness tests*

Micro-hardness measurements were performed to identify and quantify hardening or softening phenomena, from hole boundaries (penetration channel) to undeformed plate areas. The hardness was measured using an FT Microhardness Tester FM700 with 100 g load according to ISO 6507-01:2005(E) standard [41]. Each specimen was measured along three lines and ten measurements per line were collected. The preload was fixed for 5 s and the time test was 10 s.

Fig. 8 records the results for the 25 mm plate impacted by the two types of bullets. The distributions of the micro-hardness were collected along three lines: two close to the surfaces (thus to entry and exit holes) and a third along the median lines. Steel core projectiles induce a constant trend, with no substantial variation both along the three lines and along each line from the penetration channel towards the core of the plate (Fig. 8a). These values give an average hardness result of about 110–115 HV in accordance with [42]. This stable trend (in the absence of an appreciable variation even very close to penetration channel) can be attributed to the high-applied strain rate and the high temperature (demonstrated by the microstructural deformation and ABS formation): the two effects work in opposite ways and balance the final result. The alterations induced by the ballistic perforation of the steel core bullet seem not to be detrimental for the plate, which appears microstructurally unaltered (no hardness variation, no ABS). The tungsten core projectile was shown to behave differently as the brass sabot slightly modifies the hardness values (Fig. 8b). The aluminium alloy hardness increases after the impact starting from the penetration channel, where lower values are present, and reaches a similar average value (115 HV) of the previous sample far

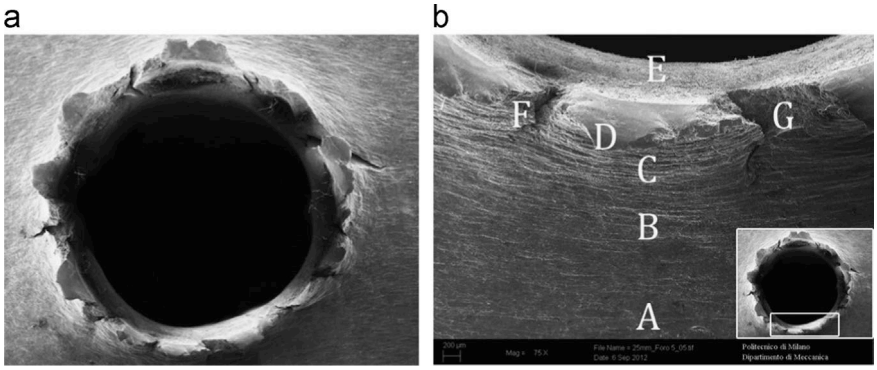

Fig. 11. SEM magnifications of the 25 mm specimen inlet hole impacted by the steel core projectile: (a) general overview and (b) investigated zones.

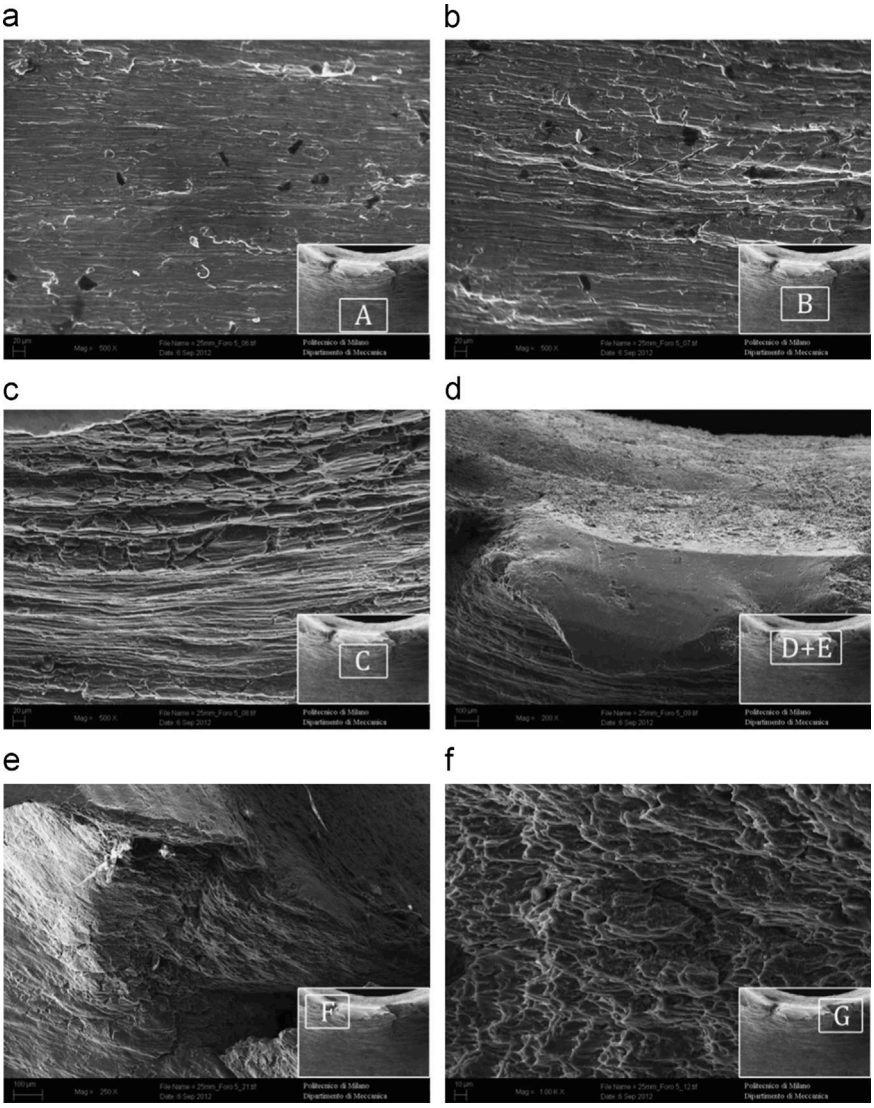

Fig. 12. 25 mm specimen entry hole due to steel core projectile at 2000× SEM magnification; refer to Fig. 11 for the position of the points.

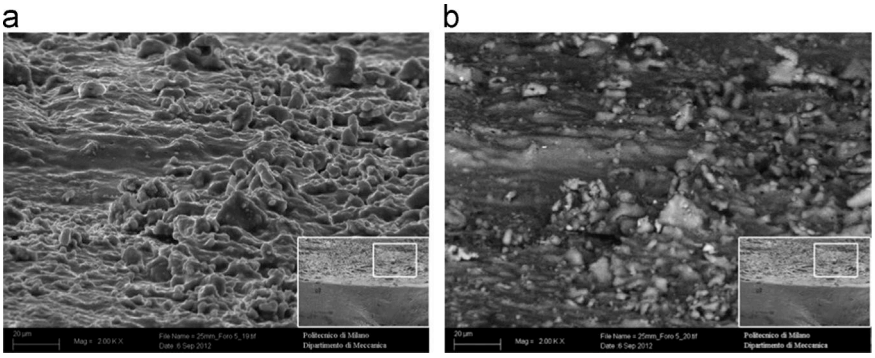

Fig. 13. Entry hole of the 25 mm specimen impacted by the steel core projectile (zone E of Fig. 11): (a) SEM image and (b) back scattered electron image.

from the damaged area. This behaviour is more pronounced in the area of the sabot (lines Db and Dc, Fig. 8b) due to the confined heat, developed during the impact by the deformation and the arrest of the sabot. This heat causes the material softening in the first area near the hole's edge, highlighted by the formation of ABS (Fig. 7).

A similar behaviour was found in the 76.2 mm specimen impacted by the tungsten carbide core projectile and in the 101.6 mm plate impacted by the steel core projectile (Fig. 9).

The 76.2 mm thickness plate impacted by the tungsten carbide core is characterised by great material softening near the penetration channel edge, passing from about 90 HV to a mean value of

116 HV along a 400 μm line. Again this phenomenon is slightly more pronounced for the line Sc, as shown in Fig. 9a, thus in the presence of the sabot. However in this case the differences between the lines are not so enhanced as for the 25 mm plate (Fig. 8b). A potential explanation lies in the very low heat conductivity of tungsten, resulting in the confinement of the major part of the heat energy generated by the impact to the hole and its absorption by the Al6061-T6.

Identical modifications have been found in the 101.6 mm plate impacted by the steel core projectile, but with a lower softening effect, due to the higher conductivity of steel if compared with tungsten.

The identical behaviour of all the plates that have stopped the projectile confirms that the softening is caused by the confined heat between the bullet and the alloy, which is also associated with the formation of the *adiabatic shear bands*.

Micro-hardness tests were also carried out on the projectile material. In this case analyses were performed to identify the material characteristics and the possible modification of these features during the impact. In the tungsten projectile the measurements identify a constant trend in hardness in the whole core. The measured mean hardness value determined on the tungsten core before impact is 1317 HV. Such a high value is consistent with the very low deformation of this component during the impact phenomena. Instead, the brass sabot of the same AP projectile points out two areas featured by different values. The undeformed zone, marked with A in Fig. 10, is characterised by the typical hardness value of the alloy CuZn30 of about 139.3 HV. On the contrary, the deformed zone B is characterised by a higher hardness value of 197.7 HV due to the hardening undergone by the alloy during the impact. High strain and high strain-rate caused in the material produce an important change in the mechanical characteristics.

The micro-hardness tests for the AP steel projectile show a very high mean hardness value of 695 HV for this alloy, which is however lower than the tungsten value. It is consistent with the absence of deformation observed in this projectile even after the impact.

4.3. SEM examination of entry and exit holes morphology

A scanning electron microscopy (SEM) survey has been performed to study the hole morphology and specifically the features associated with the modifications taken place during the impact (fusion, fracture, petalling, etc). The cavity is cylindrical and regular in the majority of the tests, with the exception of the 25 mm and 76.1 mm plates impacted by a tungsten carbide core bullet, where the brass sabot deformation is evident (Fig. 3). However, in all the tests, ductile dimples growth is the predominant failure mode. During impact and perforation, the alloy in front of the projectile is pushed out laterally with the onset of failure in terms of circumferential and radial cracks. This causes the petalling phenomena. Analyses have been mainly focused on the 25 mm plate due to the presence of the entry and exit holes allowing the study of a complete penetration channel. 25 mm plates have been analysed, starting from the impact region produced by the steel core bullet. The entry hole features an evident ductile hole enlargement with a clear petalling phenomena, see Fig. 11a. At higher magnifications, the different material behaviour in the adjacent impact area is clearly visible: far from the hole (near point A in Fig. 12a) at 3 mm from the edge of the hole, the material appears unaltered and unaffected by modification. Moving towards the edge of the penetration channel, a progressive material compression was identified, as observed by the progressive striped effect. Point B and point C (Fig. 12b and c) show initial material lacerations, probably affecting only the surface layer. In points D and E, of Fig. 12d, the alloy behaviour is

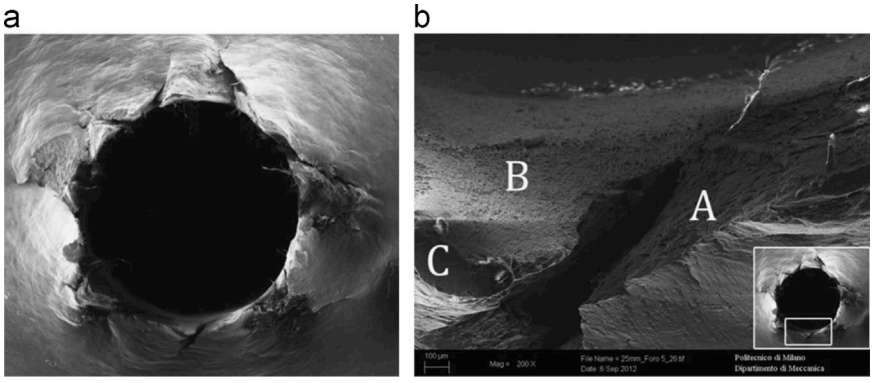

Fig. 14. Exit hole of the 25 mm specimen impacted by the steel core projectile.

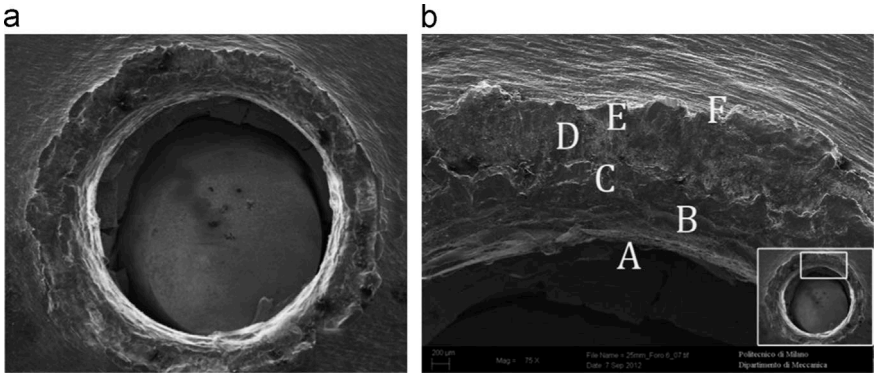

Fig. 15. Entry hole of the 25 mm specimen impacted by the tungsten core projectile.

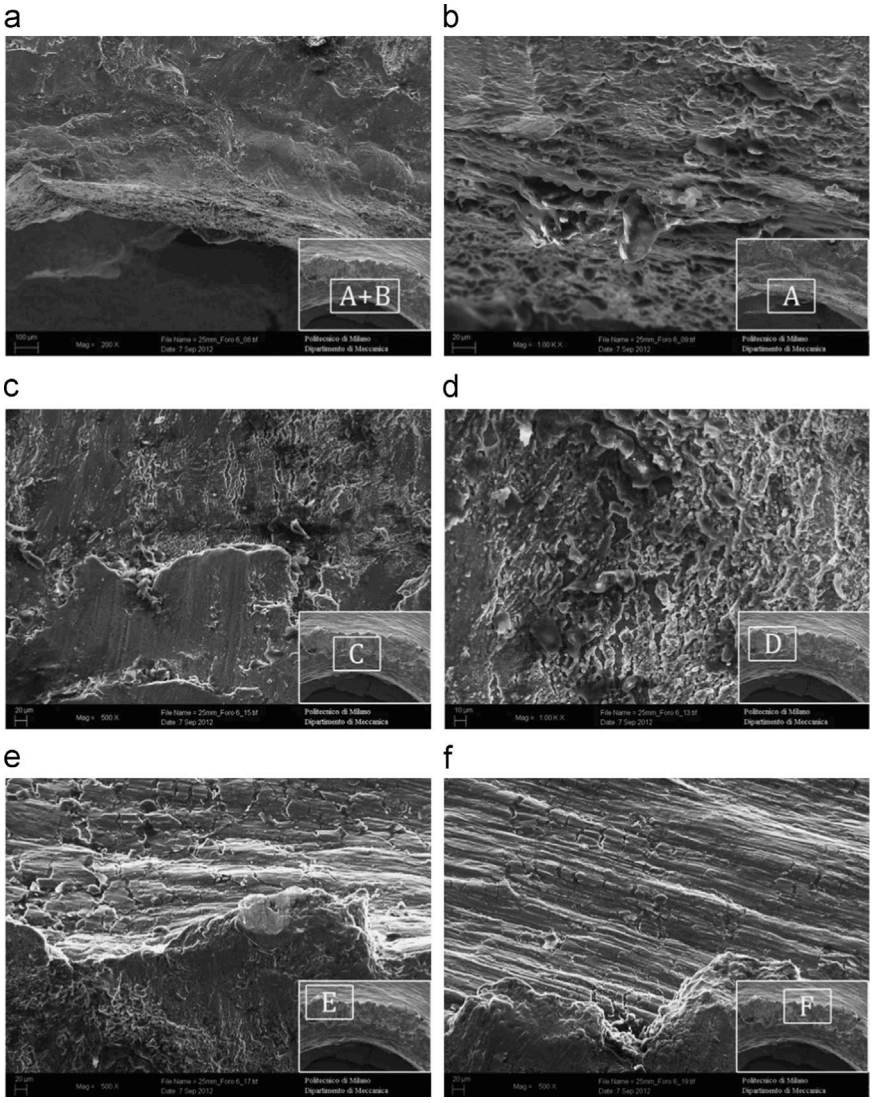

Fig. 16. Magnifications of the 25 mm specimen entry hole impacted by the tungsten core projectile; refer to Fig. 15 for the position of the points.

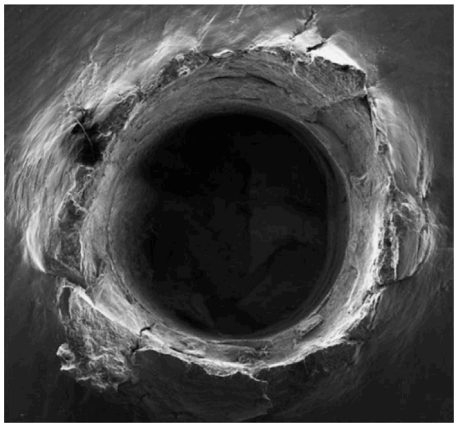

Fig. 17. Exit hole of the 25 mm specimen impacted by the tungsten core projectile.

different. The first area, D, is smooth and has a curved surface towards the outside of the petalling region, with a clear compression of the material. Point E points out a melting surface inside the hole, caused by the thermal energy dissipation originated by the

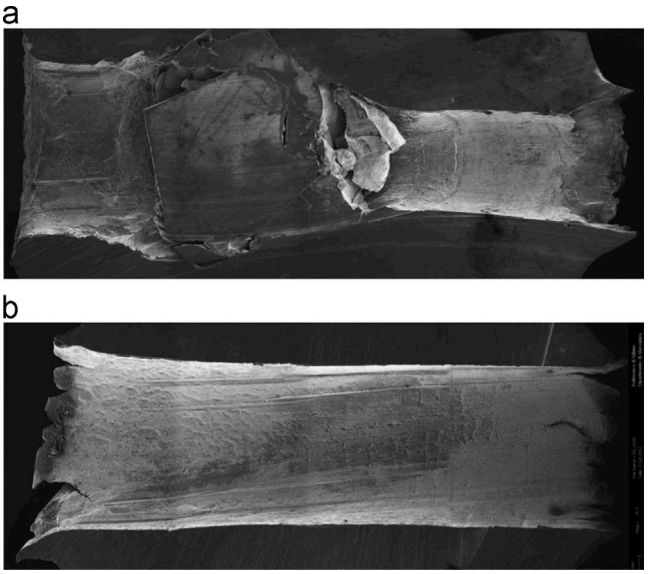

Fig. 18. Section views of the 25 mm plate penetration channel: (a) tungsten carbide core projectile and (b) steel core bullet.

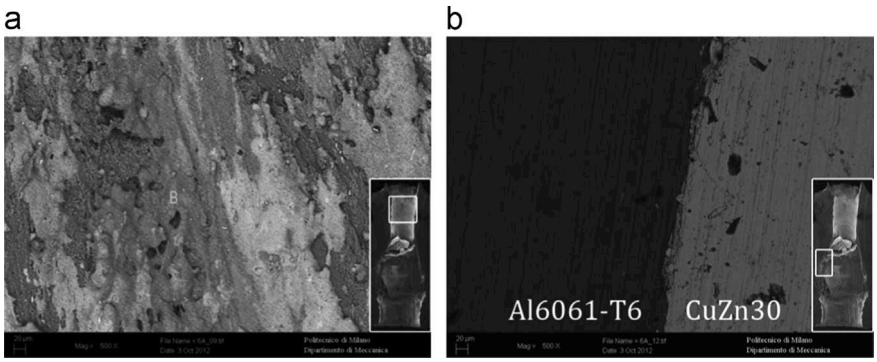

Fig. 19. BSE microscopic analyses of the 25 mm specimen impacted by the tungsten core projectile: (a) exit surface, (b) sabot and plate contact.

Table 4
Chemical analysis of the 25 mm plate outlet impacted by the tungsten core projectile.

Chemical element	Zone Fig. 19a [%]	Zone Fig. 19b [%]
Al	54.77	82.16
Cu	23.78	9.51
Mg	0.68	0.81
Zn	14.72	7.51

friction effect between the bullet surface and the base alloy. The high temperature and the following cooling step cause the re-solidification of the Al6061-T6. The same area was further analysed by back scattered electron (BSE) microscopy, see Fig. 13, allowing the identification of some projectile material particles, mainly constituted by Fe, Cu and Pb (light dots in the picture). However, the size of the particles derived from the projectiles is negligible, so the recovered bullet appears substantially undeformed.

Finally the surface separating two consecutive petals (points F and G of Fig. 12) is analysed in order to study the Al6061-T6 fracture mechanism. The fracture is characterised by ductile behaviour, as confirmed by the dimples, in addition to a marked circumferential material stretching.

The same considerations are valid for the exit side of the impacted hole (Fig. 14). In the area indicated by the letter A the ductile dimples have been formed within the ASB through the nucleation and coalescence phenomenon. Generally dimple formation is followed by fracture. Zone B exhibits clear traces of aluminium melting caused by the temperature increase generated by the energy dissipation between the bullet and the plate. Zone C consists of a smooth surface, curved towards the outside of the hole, similar to the petal crest on the inlet side of the hole. Plates impacted by the steel core bullets show identical results (data not shown).

On the other hand, the entry hole morphology of the 25 mm plate impacted by the tungsten carbide core projectile shows a different behaviour after the bullet crossing (Fig. 15). The main modality of penetration is ductile hole enlargement combined with much limited petalling. The interaction between the sabot and the aluminium implies the melting of the aluminium alloy ($T_{m,\ aluminium}$=925 K [42]) and the arrest of the brass sabot ($T_{m,\ brass}$=1189 K [43]). The melting of the plate material during the projectile penetration causes a shift of the melted plate material towards the outside hole. The plate is characterised by a wide melted region at the projectile entry area that extends up to the external hole edges (point A in Figs. 15 and 16). Moving up from point C to E in Fig. 15 the aluminium alloy appears to be constituted of two overlapping layers, melted and then re-solidified along the radial direction. As in the previous specimen the most external area (point F in Figs. 15 and 16) shows a surface layer fragmentation due to the stress fields generated by the bullet impact. However the petalling phenomenon is different compared with the steel core bullet: the melting effect seems to override the petalling formation.

On the contrary, the exit hole generated by the tungsten carbide core bullet (Fig. 17) impact shows a behaviour similar to the other steel impactor that produces petalling formation. Thus, the observed differences in the entry hole are due to the presence of the deformable brass sabot and its interaction with the aluminium target.

4.4. SEM examination along the penetration channels

An analysis of the penetration channels has been performed to examine the interactions between the Al6061-T6 alloy and the bullets. Fig. 18a shows the 25 mm specimen impacted by the tungsten carbide core projectile. As previously reported and discussed the bullet sabot remains inside the hole and thereby causes widespread modifications in the microstructure and thus hardening behaviour of the material. The analysis performed by BSE mode highlights the presence of a high residual Cu content in the penetration channel after the arrest of the sabot (Fig. 19a). The chemical composition of the Cu enriched penetration area is reported in Table 4. However, no melting between the sabot and aluminium is identified and thus no Cu diffused in the aluminium zone in Fig. 19b. The temperature reached at interface between the brass and aluminium is therefore not sufficiently high to promote the melting of the brass alloys, but is high enough to soften the Al6061-T6. The brass residue identified in the penetration channel of the only tungsten carbide core, see Fig. 19a, is most likely deposited following the detachment of the sabot from the tungsten core. The morphology of the tungsten carbide core bullet entry hole is conditioned by ductile hole enlargement and the interaction between the sabot and the hole forming surface. The plate behaviour observed is highly influenced by friction and differs between the thicknesses (Fig. 3): the 101.6 mm plate shows an additional ricochet effect of the projectile compared with the 25 mm and 76.2 mm plate. Furthermore the bullet remains undeformed in the 101.6 mm plate. This lack of deformation is most likely caused by the formation of a substantial melting aluminium film that prevents the sabot from interacting with the aluminium causing huge deformation.

The SEM analysis of the 25 mm plate impacted by the steel core projectile shows streaks left by the bullet revolution motion due to the barrel rifling (Figs. 18b 20a). The entry and exit holes show an equally large amount of petalling.

Traces of copper particles derived from the jacket of the 7.62 steel core bullet are visible at the bullet entrance area of the hole, see Fig. 20b. The chemical analysis of identified particles is

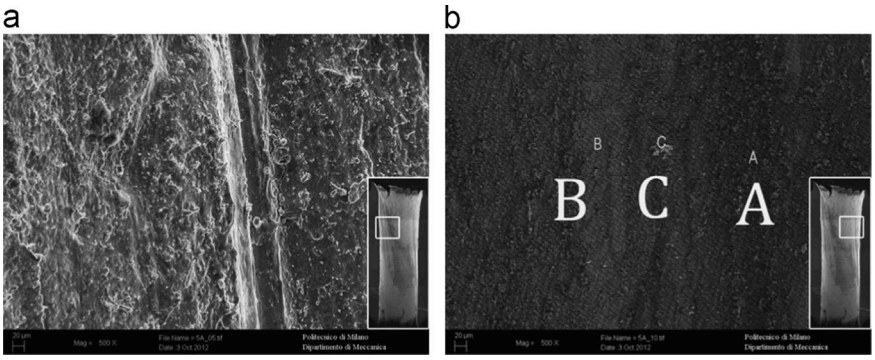

Fig. 20. Magnifications of the 25 mm specimen impacted by the steel core projectile: (a) rifling, (b) BSE analysis in the rifling zone, presence of Cu in point c (b).

Table 5
Chemical analysis of the 25 mm specimen impacted by the steel core projectile.

Chemical element	Point A [%]	Point B [%]	Point C [%]
Al	83.85	87.54	50.99
Zn	11.12	11.05	18.05
Si	2.27	1.41	3.06
Cu	1.71	–	26.92
Mg	1.03	–	–

reported in Table 5. Points A and B have similar concentrations of various chemical elements, whereas point C shows a high concentration of Cu, derived from residuals of the jacket. These results have been confirmed also for the other two plate thicknesses (data not shown).

However, the analysis of the two penetration channels in the 25 mm plate, see Fig. 18, shows other clear differences: the steel core induces a cylindrical penetration channel at the exit zone whereas the tungsten carbide bullet penetration channel is irregular after the brass sabot arrest. Its penetration channel is clearly enlarged in the exit zone and an evident plug has been recovered after the test, see Fig. 21. The presence of a plug clearly indicates a dominant failure mode characterised by ASB. However the internal surface of the exit hole produced by the tungsten carbide core shows both melted material (see Fig. 22b point N) and brittle fracture (see Fig. 22b points L, M) probably due to a localised mechanical failure driven by high strain rate and a reduction of ductility connected to the shape of the impactor. This behaviour was not observed in the steel core bullet whose ogival shape promotes a more ductile morphology of failure (Fig. 14).

The effect of friction calls for a more detailed discussion. In all the specimens analysed, the inner surfaces of the penetration channel are characterised by a more or less wide area in which the material has been melted and dragged by the projectile displacement. The present investigations confirm the presence of a thin layer of melted material in the penetration area of thick aluminium targets. It is worth mentioning that the local increase of temperature in the penetration channel is not only due to friction but also due to adiabatic heating caused by the conversion of a part of plastic deformation into heat. According to Børvik et al. [1] the kinetic frictional coefficient for aluminium on steel is 0.47, but the effect of the heat developed between the projectile and the target decreases the frictional effect to almost zero [1,6,8,44], because of the formation of a melted liquid film. Generally, numerical models of ballistic impact are carried out without any friction effects in the contact area and such an assumption seems to be correct due to the thin layer of the melted material formed in the early stage of the penetration channel as illustrated in the previous analyses. Moreover Fig. 4 shows the presence of a thin

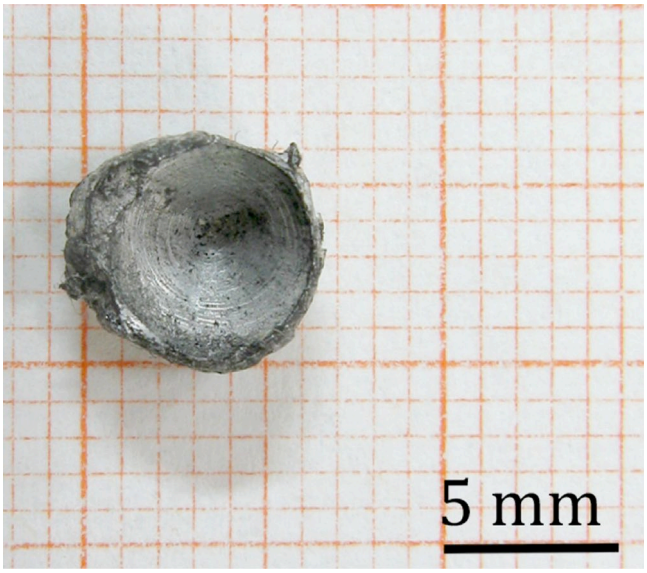

Fig. 21. Plug of Al6061-T6 recovered from the 25 mm plate impacted by the tungsten core bullet.

layer of melted aluminium on the bullets recovered from the experimental tests. For the steel core bullet the melting surface is evident in the whole penetration channel, entry (Fig. 13) and exit (Fig. 14) holes and the presence of Al on the recovered bullet (from 25 mm impact is evident in Fig. 4). The analysis of the steel core bullet composition on the 101.6 mm specimen reveals the presence of melted aluminium both on the core and on the jacket: the BSE analysis permits the identification of the presence of typical Al6061-T6 chemical composition, shown by the darker areas in Fig. 23.

For the tungsten carbide bullet the melting effect is very evident for the entry hole, see Fig. 15, where the petalling phenomena are dominated by the melting effect, and less evident in the exit hole. In this case the plugging effect has an important role in the failure surface description.

Impacts obtained by the tungsten carbide bullet against 101.6 mm result in an unusual behaviour with no deformation of the bullet and a ricochet effect of the bullet itself with a rebound velocity of 67 m/s. Fig. 24 depicts the overall penetration channel and a detail of its final part. The area indicated by the letter A, near the end of the hole, shows that the material was subjected to typical ductile fracture, stretched back by the bullet. The tip region is not exactly conical (as the tip of the bullet) but is smoother, which confirms that when the tungsten carbide core bullet penetration inside the bulk material is also driven by ductile hole enlargement. In area B, re-solidification of the target plate alloy

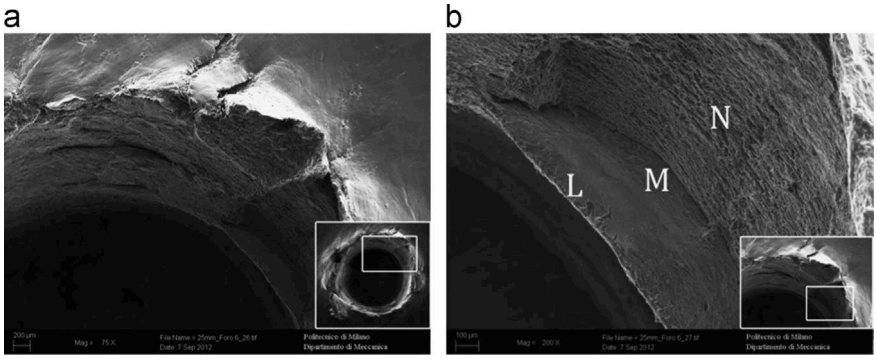

Fig. 22. Magnifications of the 25 mm exit hole provoked by the tungsten core projectile: (a) petal and (b) fracture surface after the plug detachment.

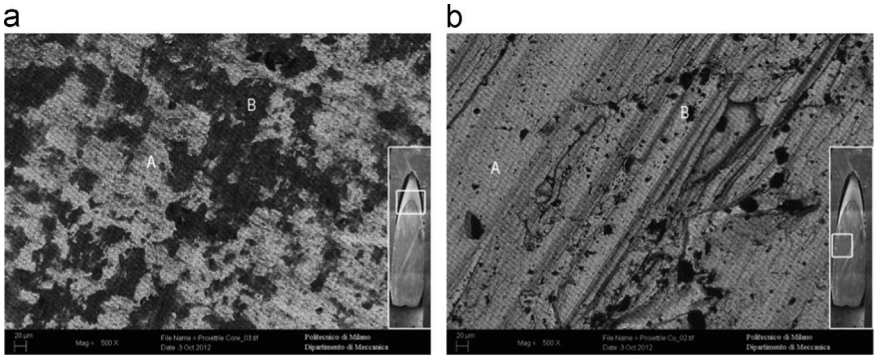

Fig. 23. BSE analyses of the 101.6 mm specimen impacted by the steel core projectile: (a) presence of melted aluminium on the core and (b) on the jacket.

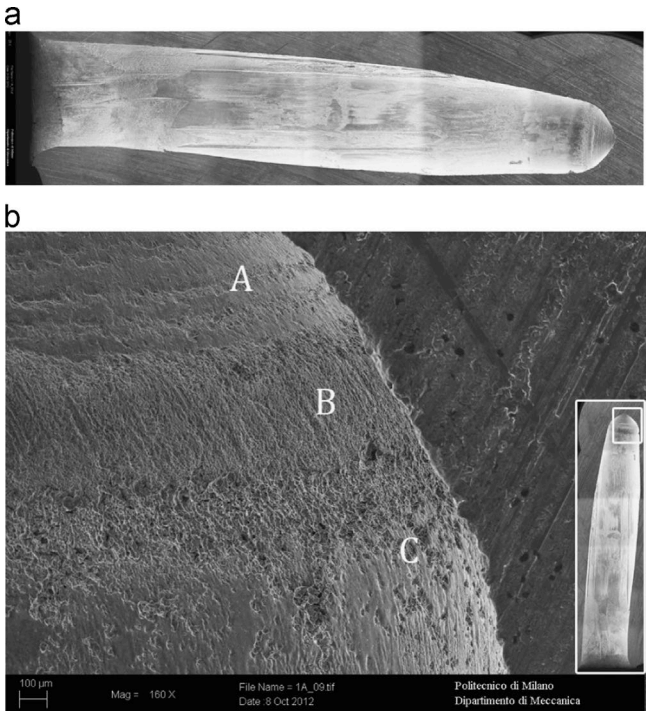

Fig. 24. Magnification of the 101.6 mm specimen impacted by the tungsten core projectile.

has taken place, associated with the presence of aluminium solid drops; area C shows identical behaviour of the other plates, with the morphology composed by melted and stretched material.

From a phenomenological point of view the effect of friction drives the impact phenomena in two different ways. For all the steel core bullet impacts and for the tungsten carbide core impact of the 101.6 mm plate the melting film drives the effect. A film of welded material is created around the bullet in the first stage of penetration, see Fig. 24 point A, and this allows the bullet to penetrate without deformation. On the contrary for the tungsten carbide core the impact (25 and 76.2 mm) friction between brass and aluminium is very pronounced and the onset of a welded film appears insufficient to allow smooth penetration of the bullet (at least for the brass part) that starts to interact with the aluminium surface and deforms it. Thus, in a numerical modelling framework the reduction of the frictional phenomena of almost zero could be reasonable only for undeformable bullet cases. On the contrary the brass sabot seems very prone to preserve a frictional effect with the aluminium provoking huge deformations.

5. Conclusions

Based on the results obtained during the analysis of the ballistic impact of different projectiles on Al6061-T6 plates, the following key points can be defined:

- The visual observation gives information about the types of damage caused by the two different projectiles in terms of surface petalling: both bullets exhibit ductile hole enlargement failure behaviour. However the melting effect of the brass sabot of the tungsten core bullet overcomes the tearing effect of the petalling.
- The metallographic analysis on the Al6061-T6 alloy shows that the microstructure modification is associated with a change in orientation and the creation of adiabatic shear bands and this phenomenon is typical of deformation characterised by high strain rate and high increase in temperature; the tungsten carbide core bullet shows a larger population of ASB due to the high deformation of the brass sabot that provokes high localised increase in temperature. It is worth mentioning that the

ASB may promote the development of cracks and can thus be dangerous in case the structure impacted is subsequently loaded.

- The micro-hardness tests have pointed out large softening when the bullet does not pierce the entire thickness. A different scenario has been found for the 25 mm specimens damaged by the steel core bullet. The interaction between the plate and the bullet is less detrimental for the plate when the projectile crosses the thickness and exits.
- The SEM examination provides important information concerning the Al6061-T6 alloy morphology obtained after the high velocity impact. The kinetic energy, owned by the projectile, is dissipated during the collision mainly in two different ways: one part drives the plastic deformation (hole enlargement, petalling, adiabatic shear bands) and as a consequence also results in an increase in temperature due to conversion of plastic work into heat; the second part is directly dissipated in friction effect as heat; this effect seems more pronounced in the tungsten carbide core bullet. Both the effects create the instant melting of the alloy, which is then re-solidified on the internal surface of the hole.
- The tungsten core bullet transfers more thermal energy to the Al6061-T6 plates, as indicated by the petalling absence and by the more pronounced microstructural alterations associated with plastic strains. Moreover, in case of the tungsten core bullet the softening affects a larger material area if compared with the steel core bullet. The tungsten core projectile seems more detrimental for the structural integrity of Al6061-T6 plates.

References

[1] T. Børvik, A.H. Clausen, O.S. Hopperstad, M. Langseth, Int. J. Impact Eng. 30 (2004) 367–384.
[2] M.J. Forrestal, A.J. Piekutowski, Int. J. Impact Eng. 24 (2000) 57–67.
[3] N.K. Gupta, M.A. Iqbal, G.S. Sekhon, Int. J. Impact Eng. 32 (2006) 1921–1944.
[4] M.J. Forrestal, T. Børvik, T.L. Warren, Exp. Mech. (2010)1245–1251.
[5] T. Børvik, M.J. Forrestal, T.L. Warren, Exp. Mech. 50 (2010) 969–978.
[6] T. Børvik, M.J. Forrestal, O.S. Hopperstad, T.L. Warren, M. Langseth, Int. J. Impact Eng. 36 (2009) 426–437.
[7] N.K. Gupta, M.A. Iqbal, G.S. Sekhon, Int. J. Solids Struct. 44 (2007) 3411–3439.
[8] M.A. Iqbal, S.H. Khan, R. Ansari, N.K. Gupta, Int. J. Impact Eng. 54 (2013) 232–245.
[9] K.A. Dannemann, C.E. Anderson Jr., G.R. Johnson, in: D.R. Leseur, T.S. Srivatsan (Eds.), Modeling the Performance of Engineering Structural Materials II, TMS, 2001, pp. 63–75.
[10] G.M. Owolabi, A.G. Odeshi, M.N.K. Singh, M.N. Bassim, Mater. Sci. Eng. A 457 (2007) 114–119.
[11] S.N. Medyanik, W.K. Liu, S. Li, J. Mech. Phys. Solids 55 (2007) 1439–1461.
[12] T.W. Wright, The Physics and Mathematics of Adiabatic Shear Bands, first ed., University Press, Cambridge, 2002.
[13] B. Bhav Singh, G. Sukumar, A. Bhattacharjee, K. Siva Kumar, T. Balakrishna Bhat, A.K. Gogia, Mater. Des. 36 (2012) 640–649.
[14] H.A. Salem, W.M. Lee, L. Bodelot, G. Ravichandran, M.A. Zikry, Metall. Mater. Trans. A 43 (2012) 1895–1901.
[15] W.M. Lee, M.A. Zikry, Metall. Mater. Trans. A 42A (5) (2011) 1215–1221.
[16] A. Manes, F. Serpellini, M. Pagani, M. Saponara, M. Giglio, Int. J. Impact Eng. 69 (2014) 39–54.
[17] Y.u.V. Milman, S.I. Chugunova, I.V. Goncharova, V.A. Goncharuk, N.A. Yefimov, Int. J. Impact Eng. 33 (2006) 452–462.
[18] A. Gilioli, A. Manes, M. Giglio, in: Proceedings of the 4th International Conference on Advanced Computational Engineering and Experimenting, ACE-X, 8–9 July 2010, Paris.
[19] A. Manes, L. Peroni, M. Scapin, M. Giglio, Procedia Eng. 10 (2011) 3477–3482.
[20] D.R. Lesuer, G.J. Kay, M.M. LeBlanc, Modeling large-strain, high rate deformation in metals, Technical Report UCRL-JC-134118, Lawrence Livermore National Laboratory, Livermore, 2001.
[21] O.S. Lee, M.S. Kim, Nucl. Eng. Des. 226 (2003) 119–125.
[22] K. Sakino, J. Soc. Mater. Sci. Jpn. 55 (11) (2006) 1021–2026.
[23] R.R. Ambriz, C.C. Froustey., G. Mesmacque, Int. J. Impact Eng. 60 (2013) 107–119.
[24] T. Børvik, A.H. Clausen, O.S. Hopperstad, M. Langseth, Int. J. Impact Eng. 36 (2009) 426–437.
[25] A.J. Piekutowski, M.J. Forrestal, K.L. Poormon, T.L. Warren, Int. J. Impact Eng. 23 (1999) 723–734.
[26] MIL-STD-662F, V5' Ballistic Test for Armour, Department of Defense Test Method Standard, 1987.
[27] S.J. Bless, D.T. Berry, B. Pedersen, S. Satapathy, T.L. Warren, W. Lawhorn, in: Proceedings of the 25th International Symposium on Ballistics, China, 2010, pp. 1339–1346.
[28] J. Newby, K. Mills, American Society for Metals, ASM Handbook Volume 09: Metallography and Microstructures, ninth ed., ASM International, Ohio (2004) 2004694–1688.
[29] AA.VV., ASM Metal Handbook, Vol. 4, Heat Treating, ASM International, Materials Park, OH, 1995.
[30] AA.VV., ASM Metal Handbook, Vol. 9, Metallography and Microstructure, ASM International, Materials Park, OH, 2004.
[31] M.H. Farshidi, M. Kazeminezhad, H. Miyamoto, Mater. Sci. Eng. A 580 (2013) 202–208.
[32] E. Linardi, R. Haddad, L. Lanzani, Procedia Mater. Sci. 1 (2012) 550–557.
[33] A.O. Adesola, A.G. Odeshi, U.D. Lanke, Mater. Des. 45 (2013) 212–221.
[34] C. Zener, J.H. Hollomon, J. Appl. Phys. 15 (1) (1944) 22–32.
[35] A. Merzer, J. Mech. Phys. Solids 30 (5) (1982) 323–338.
[36] T.W. Wright., The Physics and Mathematics of Adiabatic Shear Band. Cambridge Monographs on Mechanics, Cambridge University Press, Cambridge, 2002, ISBN: 9780521631952.
[37] D.H. Li, Y. Yang, T. Xu, H.G. Zheng, Q.S. Zhu, Q.M. Zhang, Mater. Sci. Eng. A 527 (15) (2010) 3529–3535.
[38] H. Berns, S. Riedner, V. Gavriljuk, Y. Petrov, A. Weihrauch, Mater. Sci. Eng. A 528 (2011) 4669–4675.
[39] T. Børvik, A.H. Clausen, M. Eriksson, T. Berstad, O.S. Hopperstad, M. Langseth, Int. J. Impact Eng. 32 (2005) 35–64.
[40] Y.B. Xu, J.H. Zhang, Y.L. Bai, M.A. Meyers, Metall. Mater. Trans. A 39 (2008) 811–843.
[41] ISO 6507-01:2005(E), Metallic Materials – Vickers Hardness Test – Part 1: Test Method, third ed., International Standard, 2005.
[42] G.E. Totten, D.S. MacKenzie, Handbook of Aluminium Volume 1: Physical Metallurgy and Processes, first ed., CRC Press, New York, 2003.
[43] J.R. Davis, ASM Speciality Handbook: Copper and Copper Alloys, first ed., ASM International, 2001.
[44] M.J. Forrestal, K. Okajima, V.K. Luk, J. Appl. Mech. 55 (1988) 755–760.